International Journal of Pioneering Technology and Engineering

Research Article

Effect of inner channel geometry on solidification performance of phase change material (PCM) in double-pipe thermal energy storage

Burak Kurşun [a*] **Mehmet Balta**[b]

[a] Faculty of Engineering, Mechanical Engineering Department, Amasya University, Amasya, Turkey,

[b] Technical Sciences Vocational School, Machinery and Metal Technologies Department, Amasya University, Amasya, Turkey,

Article Info

Article history
Received: 27/10/2023
Revised: 14/11/2023
Accepted: 02/12/2023

Keywords:
Double pipe,
PCM,
Solidification

ABSTRACT

Advantages such as high energy storage density and low heat losses have made phase change materials (PCMs) preferable in energy storage. However, the very low thermal conductivity of PCMs is the most important obstacle to improving melting and solidification performance of PCMs. To improve the thermal conductivity of PCM, the combination of PCM with nanoparticles, fins, and metal foam is among the methods widely researched in the literature. The innovation of this study was to examine the effect of inner and outer channel configurations on the solidification rate in double-pipe energy storage with PCM. Thus, it was aimed to benefit from the same amount of stored energy more and at a lower cost. In this regard, solidification analyses were carried out for three different basic inner channel geometries. With the triangle-in-circle configuration, the solidification rate was increased by 5.5% to 13.2% compared to other configurations. It is anticipated that the data obtained in this study will be a guide for novel inner channel geometry designs that will increase solidification performance and heat transfer in double-pipe energy storage with PCM.

1. Introduction

Increasing fossil fuel use has led to environmental problems such as air pollution and global warming. In order to use energy efficiently, it is important to store thermal energy obtained from renewable and clean energies. One of the energy storage methods is latent heat storage. Energy can be stored in phase change materials (PCMs) with high storage capacity. PCMs store energy during melting (charge time) and give back the stored energy during solidification (discharge time). Due to their low coefficient of thermal conductivity, PCMs have long charge and discharge times. The negative feature of PCM is its low thermal conductivity and to overcome this disadvantage, it is aimed to reduce the charge and discharge times by using it in combination with fins, nanoparticles, or metal foam [1,2].

Double-pipe thermal energy storage (DPTES) is the preferred structure for energy storage with PCM due to its simple and compact structure. The methods mentioned above to improve the thermal conductivity of PCM (fins, nanoparticles or metal foam) have also been used in DPTES. An important problem in the use of nanoparticles is that the particles cannot be distributed homogeneously enough and agglomeration occurs between the particles. In the use of fins and metal foam, there are disadvantages such as decreased energy storage capacity and increased system costs. In order to eliminate these disadvantages and reduce system costs, the use of channels with different geometries in the DPTES is a more appropriate solution. Studies on different internal and external duct geometries in SPPPES are quite limited. Mahdi et al. and Nafajabadi et al. obtained an increase in melting performance with spiral inner tube geometry with different cross-sectional areas [3,4]. Hekmat et al. investigated the effects of vessel geometry (triangle, square, trapezoid, and ellipse), nanoparticles and fins on melting and solidification to reveal the optimum design [5]. Alnekaab et al. investigated the effects of a straight inner tube on melting performance [6]. Bazai et al. showed the effects of different sizes of elliptical inner tubes on melting and solidification rates [7]. In addition, the effects of the inner tube design with wavy surface geometry on melting and solidification performance have also been reported through studies [8-10].

In the previous study, melting analysis of different inner-outer channel geometry configurations was performed [11]. Solidification analysis was also performed for the configuration with the highest melting rate. The novelty in this study was that solidification analysis was carried out for all inner-outer channel combinations, independent of melting analysis. Thus, it was aimed to see the effects of inner-outer channel combinations, which were not tested for solidification in the previous study. In this direction, solidification analysis was carried out for three different inner-outer channel configurations and the factors affecting the change in solidification rate were tried to be determined. Analysis results were evaluated in terms of liquid fraction, solidification rate, and PCM temperature.

2. Materials and Methods

Three different inner tube geometries were used in solidification analyses. These simple main geometries were preferred because they are easy and economical to manufacture. Inner channels with circular, square, and triangular geometries are shown in Fig.1. To ensure a homogeneous heat transfer in square and triangular geometries, geometries with equal side lengths were preferred. The circle-in-circle configuration was taken as the main geometry. In other configurations, the outer pipe diameter .

***Corresponding author:** Burak Kurşun
*E-mail address: burak.kursun@amasya.edu.tr
https://doi.org/10.56158/jpte.2023.54.2.02

was kept constant, and the side lengths of triangular and square geometries were determined by considering the PCM area in the circle-in-circle combination. The edge lengths obtained for equal PCM areas are given in Table 1.

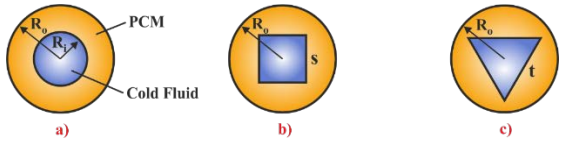

Fig 1. Inner channel geometries for DPTES

Table 1. Edge lengths of geometric configurations

Combination number	R_i (mm)	R_o (mm)	s (mm)	t (mm)	PCM Surface Area (mm^2)	Inner duct perimeters (mm)
a)	10	20	-	-	942.5	62.83
b)	-	20	17.72	-	942.5	70.88
c)	-	20	-	26.94	942.5	80.82

2.1. Mathematical Model

The enthalpy-porosity method was applied in numerical solidification analyses. The numerical solution was carried out following the assumptions given below.

- It was assumed that the computational domain was two-dimensional, the flow was time-dependent, and the fluid was incompressible and Newtonian [3].
- The Boussinesq approach was adopted for natural convection flow [6].
- Viscous dissipation was ignored [7].
- The outer pipe surface was assumed to be adiabatic [11].

Conservation of mass and conservation equations in the x and y axes directions are below.

Continuity

$$\frac{\partial \rho}{\partial t}+\frac{\partial(\rho u)}{\partial x}+\frac{\partial(\rho v)}{\partial y}=0 \quad (1)$$

Momentum in x direction

$$\frac{\partial(\rho u)}{\partial t}+\frac{\partial(\rho u u)}{\partial x}+\frac{\partial(\rho v u)}{\partial y}=-\frac{\partial p}{\partial t}+\frac{\partial}{\partial x}\left(\mu\frac{\partial u}{\partial x}\right)+\frac{\partial}{\partial y}\left(\mu\frac{\partial u}{\partial y}\right)+uA \quad (2)$$

Momentum in y direction

$$\frac{\partial(\rho v)}{\partial t}+\frac{\partial(\rho u v)}{\partial x}+\frac{\partial(\rho v v)}{\partial y}=-\frac{\partial p}{\partial t}+\frac{\partial}{\partial x}\left(\mu\frac{\partial v}{\partial x}\right)+\frac{\partial}{\partial y}\left(\mu\frac{\partial v}{\partial y}\right)+$$

$$vA+\rho g\beta(T-T_m) \quad (3)$$

In the equations, g denotes the gravitational acceleration, ρ denotes the density, β denotes the thermal expansion coefficient, T expresses the temperature, μ denotes the dynamic viscosity, u indicates the fluid velocity in the x direction and v indicates the fluid velocity in the y direction. The A value is found with the Eq. (4) [12],

$$A=-A_{mush}\frac{(1-\lambda)^2}{\lambda^3+\varepsilon} \quad (4)$$

Where λ is the liquid fraction and defined by Eq. (5) [13],

$$\lambda=\begin{cases}0 & ;\ T<T_s\\ (T-T_s)/(T_l-T_s) & ;\ T_s<T<T_l\\ 1 & ;\ T>T_l\end{cases} \quad (5)$$

where the l and s subscripts represent the liquid and the solid phase, respectively. A_{mush} indicates the mushy zone constant and was assumed to be $A_{mush}=10^5$. ε denotes the small number (ε =0.001) [12]. The energy equation is given by following equation,

Energy equation

$$\frac{\partial(\rho h)}{\partial t}+\frac{\partial(\rho u h)}{\partial x}+\frac{\partial(\rho v h)}{\partial y}=\frac{\partial}{\partial x}\left(k\frac{\partial T}{dx}\right)+\frac{\partial}{\partial y}\left(k\frac{\partial T}{dy}\right) \quad (6)$$

where k is the fluid conductivity, and h denotes the sensible enthalpy. h is determined with the Eq. (7) [13],

$$h=\begin{cases}\int_{T_{ref}}^{T}c_p\,dT & ;\ T<T_s\\ \int_{T_{ref}}^{T}c_p\,dT+\lambda \mathrm{H} & ;\ T_s<T<T_l\\ \int_{T_{ref}}^{T_s}c_p\,dT+\int_{T_l}^{T}c_p\,dT & ;\ T>T_l\end{cases} \quad (7)$$

where Tref, H, and Cp represent the reference temperature (T_{ref}=298.15 K), the latent heat, and specific heat capacity, respectively. T is calculated by following equation [14],

$$T=\lambda(T_l-T_s)+T_s \quad (8)$$

N-eicosane was used as the PCM material due to its advantages such as being commercial and easy to access. The thermal properties of the N-eicosane material are presented in Table 2.

Table 2. Thermophysical properties of N-eicosane PCM [16]

Thermophysical properties	**Value**
Solidus/ Liquidus Temperature (K)	308.15/310.15
Liquid Density (kg/m^3)	770
Specific Heat Capacity (J/kgK)	2460
Latent Heat Of Fusion (J/kg)	247600
Thermal Conductivity (W/mK)	0.1505
Thermal Expansion Coefficient (1/K)	0.0009
Dynamic Viscosity (kg/ms)	0.00385

The convection heat transfer coefficient in the inner channels (h_{conv}) was calculated by the Dittus-Boelter correlation (Eq. (9)) [17].

$$\mathrm{Nu}=0.023Re^{0.8}Pr^{0.4} \quad (9)$$

The equations given below were used to calculate the h_{conv}, Nusselt (Nu), and Reynolds number (Re).

$$Re=\frac{\rho V D_H}{\mu} \quad (10)$$

$$D_H=\frac{4A_c}{p} \quad (11)$$

$$Nu=\frac{h_{conv}D_H}{k} \quad (12)$$

where A_c is the cross-sectional area, p is the perimeter length, and h_{conv} is the convection heat transfer coefficient.

2.2 Boundary Conditions

In the analyses, the average melting temperature of PCM was taken as 309.15 K. At the beginning of the solidification analysis, the PCM temperature was 310.15 K (Eq. (13)). h_{conv} was applied on the inner surface of the inner pipe (Eq. (14)). As mentioned before, the outer pipe surface was considered adiabatic (Eq. (15)). The T_{ave}, fluid in the inner pipe was chosen as 289.15 K.

$$\mathrm{T_{PCM}}=310.15\mathrm{K},\mathrm{t(s)}=0 \quad (13)$$

$$\dot{\mathrm{q}}_{\mathrm{cond,IS}}=\mathrm{h_{conv}}(\mathrm{T_w}-\mathrm{T_{m,f}}),\mathrm{t(s)}=\mathrm{t} \quad (14)$$

$$\dot{\mathrm{q}}_{\mathrm{cond,OS}}=0,\mathrm{t(s)}=\mathrm{t} \quad (15)$$

where T_w is the wall temperature of the inner pipe, T_m, f is the average fluid temperature, IS and OS subscripts indicate the inner and outer surface of the inner and outer pipe, respectively.

2.3 Numerical Method

Numerical analyses were carried out using the commercial program ANSYS Fluent 2022R1. The PISO algorithm was used for the pressure-velocity coupling and the PRESTO! scheme was preferred for the pressure correction equation. The QUICK scheme was applied for the discretization of momentum and energy equations and the first-order implicit transient formulation

was used for the time-dependent flow analysis. In transient analyses, the convergence criteria were determined as 10^{-6} for the continuity and momentum equations and 10^{-8} for the energy equation.

A tetrahedral grid type was adopted for the numerical analyses. Since symmetrical conditions existed in the computational domain, half of the geometries were modeled for the analyses. The grid structures generated for all geometric combinations are given in Fig. 2.

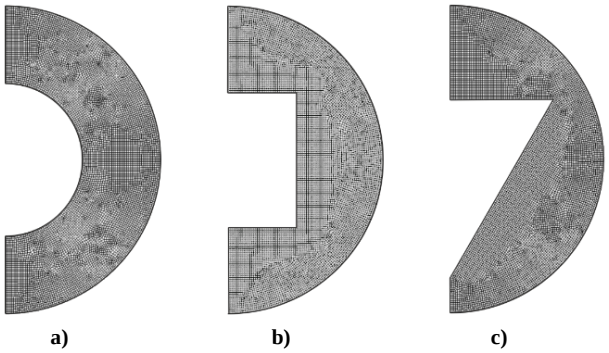

Fig. 2. Generated grid structures, a) circle-in-circle, b) square-in-circle b) triangle-in-circle

3. Results and Discussion

In this section, the effects of internal channel geometries on the solidification performance of PCM in double-pipe energy storage were evaluated in terms of liquid fraction and PCM temperature. However, beforehand, validation analyses were carried out to test the accuracy of the numerical results.

3.1 Verification Processes

For verification processes, independence tests from grid size and time step were first performed. As seen in Figure 3, the change in liquid fraction was negligible for the grid size smaller than 0.25 mm and the time step smaller than 0.15 s. Therefore, a grid size of 0.25 mm and a time step of 0.15 s were chosen for parametric analysis.

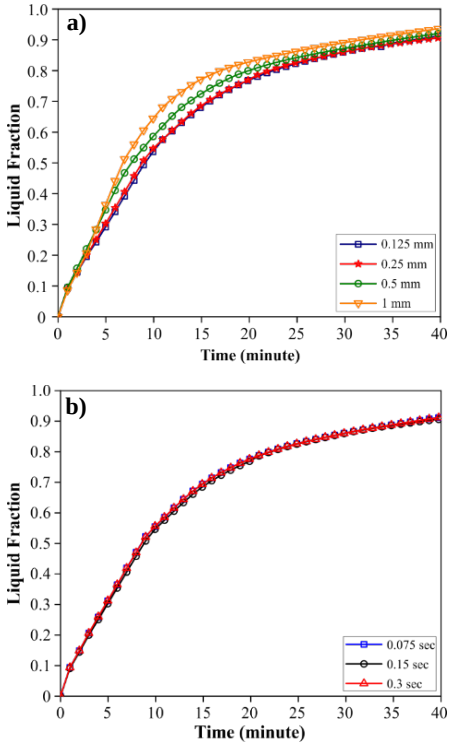

Fig. 3. Circle-in-circle configuration, a) grid size independence analysis, b) time step independence analysis

The PCM melting analysis results in the circle-in-circle configuration were validated with the results in Ref. [15]. Comparison of liquid fraction contours are given in Fig. 4a, and comparison of liquid fraction curves for the 65-minute melting period are given in Fig. 4b. The highest difference between the two analysis results was measured as 6.5%. This error rate showed that the numerical model used was applicable for a certain melting and solidification period.

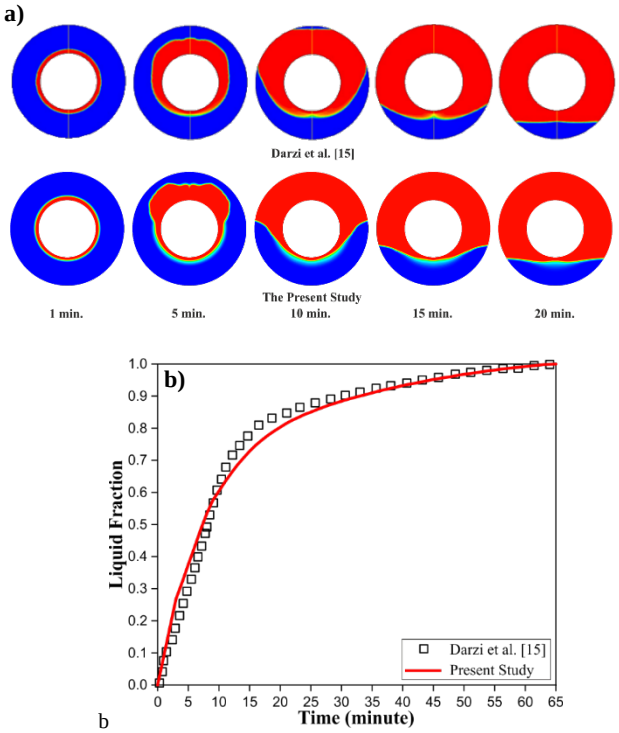

Fig. 4. Verification processes, a) liquid fraction contours, b) liquid fraction curves

3.2 Effect of Geometric Combinations on Solidification Performance

The heat transfer surface area (A_s) and the h_{conv} between the fluid in the inner pipe and the pipe surface (h_{conv}) are the main factors affecting the solidification performance. Although Nu decreased for the same water mass flow rate ($\dot{m}$=0.36 kg/s) in square and triangular geometries, h_{conv} values increased due to the decrease in DH. The highest h_{conv} value was reached in the triangular internal channel geometry (Fig. 5).

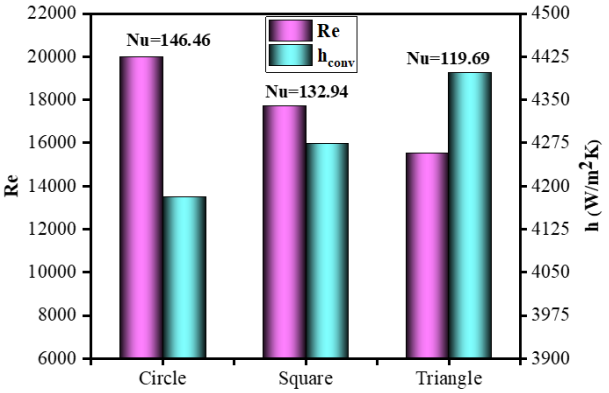

Fig. 5. Nu, Re numbers and h_{conv} depending on inner channel geometry

Fig. 6 shows the liquid fraction (LF) and temperature contours obtained for the 40-minute solidification period. In inner channel geometries, the highest perimeter length for an equal PCM area was obtained in triangular geometry. This situation increased As. As a result of an increase in As and h_{conv} for triangular geometry, the lowest temperature and liquid fraction were reached in the triangle-in-circle geometry in the 40-minute solidification period.

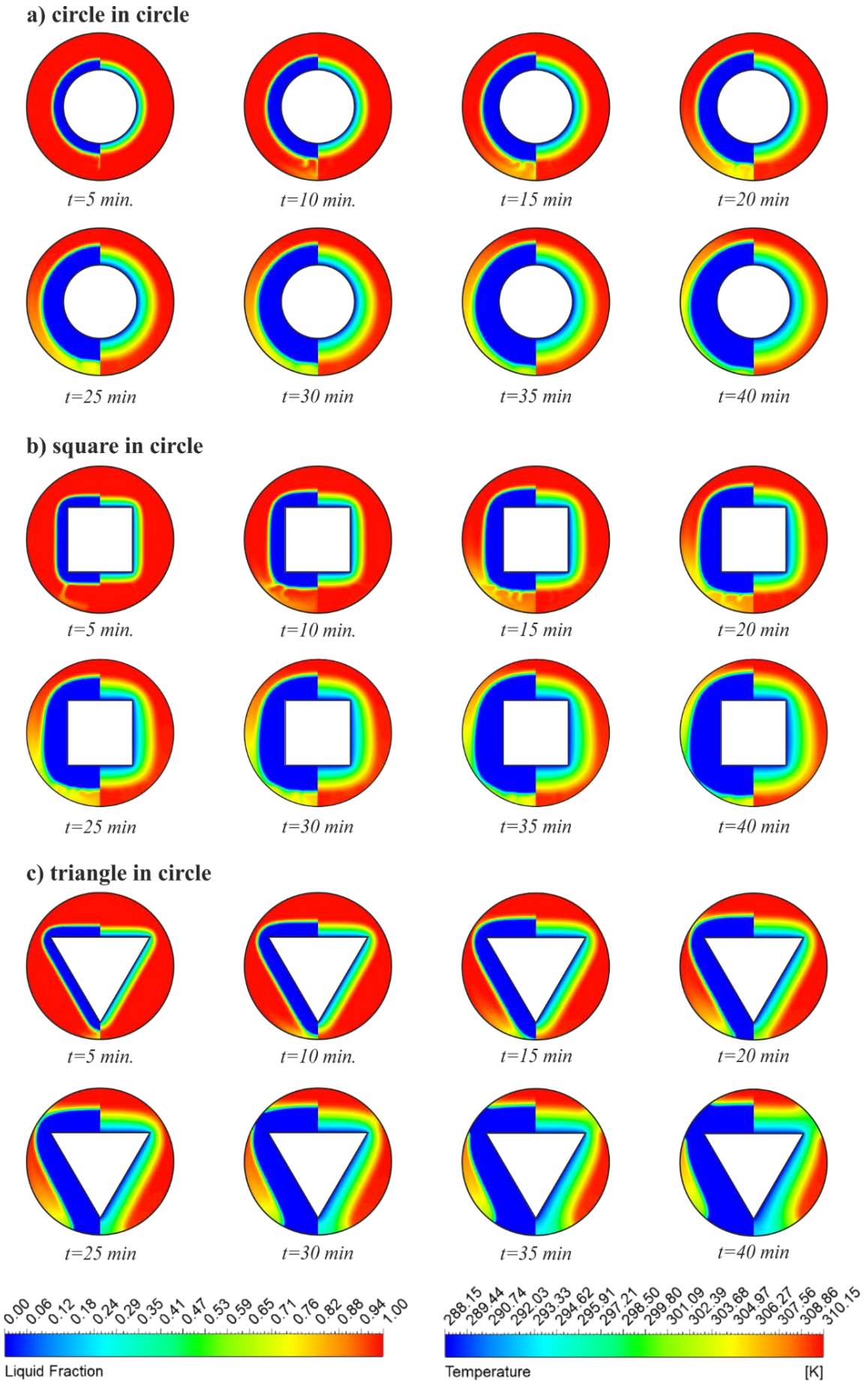

Fig. 6. Temperature (right) and liquid fraction (left) contours for different geometrical configurations in solidification process

In Fig. 7, time-dependent average PCM temperature and liquid fraction curves are presented. With the triangular inner channel geometry, the LF after 40 minutes was obtained as 0.158. According to the LF values in circular and square internal channel geometries, a decrease of 21.8% and 38.3% was achieved, respectively (Fig 7a). In other words, the solidification rate increased with the use of triangular inner channel geometry. Especially after the 10th minute, there was a significant decrease in PCM temperature in the triangle-in-circle configuration compared to the PCM temperature values in the other configurations (Fig. 7b).

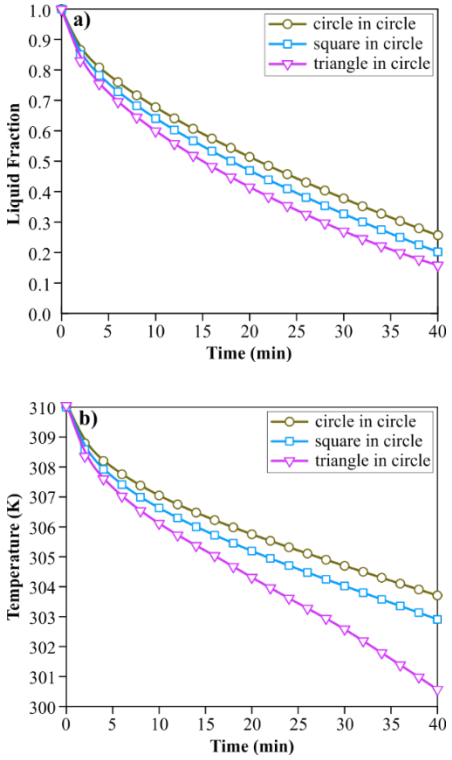

Fig. 7. Liquid fractions (a) and average PCM temperature (b) in the solidification period for all geometric configurations

4. Conclusions

In this study, the solidification performance of PCM in double-pipe energy storage was examined for three different inner channel geometries. Since solidification starts from the inner channel surface, it was observed that the most important factors affecting the solidification rate are the A_s and the h_{conv} in the inner channel. The lowest temperature and liquid fraction were attained in the triangle-in-circle geometry during the 40-minute solidification phase due to an increase in As and h_{conv} for triangular geometry. The highest h_{conv} value was reached in the triangular internal channel geometry. While Nu decreased for the same water mass flow rate ($\dot{m}$=0.36 kg/s) in square and triangular geometries, h_{conv} values increased due to the decrease in DH. It was revealed that the solidification rate could be increased by 5.5% to 13.2% with the circle-in-triangle configuration compared to configurations containing other basic geometries.

It is anticipated that the data obtained in this study will be a guide for novel inner channel geometry designs that will increase solidification performance and heat transfer in double-pipe energy storage with PCM.

Declaration of conflicting interests

The authors declare no competing interests.

Funding

The author received no financial support for the research and/or authorship of this article.

References

[1] Choure, B. K., Alam, T., & Kumar, R. “A review on heat transfer enhancement techniques for PCM based thermal energy storage system.” *Journal of Energy Storage*, 72, 108161,2023.

[2] Wu, S., Yan, T., Kuai, Z., & Pan, W. “Thermal conductivity enhancement on phase change materials for thermal energy storage: A review.” *Energy Storage Materials*, 25, 251-295,2020.

[3] Mahdi, M. S., Mahood, H. B., Mahdi, J. M., Khadom, A. A., & Campbell, A. N. “Improved PCM melting in a thermal energy storage system of double-pipe helical-coil tube.” *Energy Conversion and Management*, 203, 112238,2020.

[4] Najafabadi, M. F., Rostami, H. T., & Ganji, D. D. “Thermal and geometrical investigation of an original double-pipe helical coil heat storage system with kock snowflake cross-section containing phase-change material.” *Applied Thermal Engineering*, 226, 120244,2023.

[5] Hekmat, M. H., Haghani, M. H. K., Izadpanah, E., & Sadeghi, H. “The influence of energy storage container geometry on the melting and solidification of PCM.” *International Communications in Heat and Mass Transfer*, 137, 106237,2022.

[6] Alnakeeb, M. A., Salam, M. A. A., & Hassab, M. A. “Eccentricity optimization of an inner flat-tube double-pipe latent-heat thermal energy storage unit.” *Case Studies in Thermal Engineering*, 25, 100969,2021.

[7] Bazai, H., Moghimi, M. A., Mohammed, H. I., Babaei-Mahani, R., & Talebizadehsardari, P. “Numerical study of circular-elliptical double-pipe thermal energy storage systems.” *Journal of Energy Storage*, 30, 101440,2020.

[8] Shahsavar, A., Ali, H. M., Mahani, R. B., & Talebizadehsardari, P. “Numerical study of melting and solidification in a wavy double-pipe latent heat thermal energy storage system. *Journal of Thermal Analysis and Calorimetry*, 141, 1785-1799,2020.

[9] Shahsavar, A., Al-Rashed, A. A., Entezari, S., & Sardari, P. T. “Melting and solidification characteristics of a double-pipe latent heat storage system with sinusoidal wavy channels embedded in a porous medium.” *Energy*, 171, 751-769,2019.

[10] Shahsavar, A., Khosravi, J., Mohammed, H. I., & Talebizadehsardari, P. “ Performance evaluation of melting/solidification mechanism in a variable wave-length wavy channel double-tube latent heat storage system.” *Journal of Energy Storage*, 27, 101063,2020.

[11] Kurşun, B., & Balta, M. “Evaluation of the different inner and outer channel geometry combinations for optimum melting and solidification performance in double pipe energy storage with phase change material: A numerical study.” *Journal of Energy Storage*, 65, 107250,2023.

[12] Kadivar, M. R., Moghimi, M. A., Sapin, P., & Markides, C. N. “Annulus eccentricity optimisation of a phase-change material (PCM) horizontal double-pipe thermal energy store.” *Journal of Energy Storage*, 26, 101030,2019.

[13] Yan, P., Fan, W., Yang, Y., Ding, H., Arshad, A., & Wen, C. “Performance enhancement of phase change materials in triplex-tube latent heat energy storage system using novel fin configurations.” *Applied Energy*, 327, 120064,2022.

[14] Yang, X. H., Tan, S. C., & Liu, J. “ Numerical investigation of the phase change process of low melting point metal.” *International Journal of Heat and Mass Transfer*, 100, 899-907,2016.

[15] Darzi, A. R., Farhadi, M., & Sedighi, K. “ Numerical study of melting inside concentric and eccentric horizontal annulus.” *Applied Mathematical Modelling*, 36(9), 4080-4086,2012.

[16] Seddegh, S., Wang, X., & Henderson, A. D. “Numerical investigation of heat transfer mechanism in a vertical shell and tube latent heat energy storage system.” *Applied thermal engineering*, 87, 698-706,2015.

[17] Dittus, F. W., & Boelter, L. M. K. “Heat transfer in automobile radiators of the tubular type.” *International communications in heat and mass transfer*, 12(1), 3-22,1985.